The chemical species of mercury accumulated by *Pseudomonas idrijaensis*, a bacterium from a rock of the Idrija mercury mine, Slovenia.

Jean-Paul Bourdineaud [a, *], Goran Durn [b], Bojan Režun [c], Alain Manceau [d], Jasna Hrenović [e]

[a] *University of Bordeaux, CNRS, Fundamental Microbiology and Pathogenicity Laboratory, European Institute of Chemistry and Biology, 2 Rue Robert Escarpit, 33607, Pessac, France*
[b] *University of Zagreb, Faculty of Mining, Geology and Petroleum Engineering, Croatia*
[c] *Idrija UNESCO Global Geopark, Lapajnetova 1A 5280, Idrija, Slovenia*
[d] *University Grenoble Alpes, CNRS, ISTerre, 38000, Grenoble, France*
[e] *University of Zagreb, Faculty of Science, Department of Biology, Zagreb, Croatia*

HIGHLIGHTS

- Newly discovered bacterium *Pseudomonas idrijaensis* from a rock of the Idrija mine.
- The rock sample was rich in quartz and mica and contained 2952 mg of mercury per kg.
- *Pseudomonas idrijaensis* is resistant to 80 μM of mercury chloride (16 mg Hg/L).
- *P. idrijaensis* is endowed with the *mer* operon, contained in the transposon Tn*5041*.
- *P. idrijaensis* accumulates bis and tetrathiolate species: $Hg(SR)_2$ and $Hg(SR)_4$.

GRAPHICAL ABSTRACT
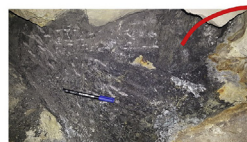
ARTICLE INFO

ABSTRACT

A mercury-resistant bacterial strain has been isolated from a rock of the Idrija mercury mine in Slovenia. The rock had 19 g carbon and 2952 mg mercury (Hg) per kg. Mass spectrometry and DNA sequencing showed that the bacterium belongs to the *Pseudomonas* genus. It is called *Pseudomonas idrijaensis*. This bacterial strain is sensitive to methylmercury (MeHg) like the reference *P. aeruginosa* strain PAO1, and is resistant to divalent mercury (Hg(II)) in contrast to PAO1. This difference could be attributed to the presence of the *mer* operon yet deprived of the *mer*B gene encoding the organomercurial lyase, on the basis of whole genome sequencing. The *P. idrijaensis mer* operon displays the RTPCADE organization and is contained in the Tn*5041* transposon. This transposon identified here occurs in other Gram-negative Hg-resistant strains isolated from mercury ores, aquatic systems and soils, including *Pseudomonas* strains from 15,000 to 40,000 years old Siberian permafrost. When *P. idrijaensis* was exposed to mercury chloride, two intracellular Hg species were identified by high energy-resolution XANES spectroscopy, a dithiolate $Hg(SR)_2$ and a tetrathiolate $Hg(SR)_4$ complex. *P. idrijaensis* had a much higher $[Hg(SR)_2]/$

* Corresponding author.
E-mail addresses: jean-paul.bourdineaud@u-bordeaux.fr (J.-P. Bourdineaud), gdurn@rgn.hr (G. Durn), bojan.rezun@ds-rs.si (B. Režun), alain.manceau@univ-grenoble-alpes.fr (A. Manceau), jasna.hrenovic@biol.pmf.hr (J. Hrenović).

$[Hg(SR)_4]$ molar ratio than bacteria lacking the *mer* operon when exposed to 4 μg Hg^{2+}/L - resulting in an intracellular accumulation of 4.3 μg Hg/g dw. A higher amount of the $Hg(SR)_2$ complex provides a chemical signature for the expression of the dicysteinate Mer proteins in response to mercury toxicity.

1. Introduction

Although mercury deposits are globally distributed in 26 mercury mineral belts, nearly three quarters of the total world's production has originated from just five mercury belts (Rytuba, 2003). Almadén, the most important mercury belt comprising 11 mercury deposits in central Spain, has produced over one-third of the world's mercury. The second largest mercury mine in the world was Idrija, Slovenia. Idrija is located about 50 km west of the Slovenian capital Ljubljana. The mine is 1500 m long and 300−600 m wide and extends below the surface of the Idrija valley in the NW − SE direction. It has produced more than 12.7 Mt of ore with 145,000 t Hg (average content of 1.13% Hg) since 1490 (Mlakar, 1974). The production of mercury stopped in 1988 and the mine finally closed in 1995. Idrija still contains 10% of the world's known mercury reserves (Brinck and van Wambeke, 1975). Idrija was considered for centuries to be the center of scientific and technological progress in the region. Mining operations in more than 150 orebodies extended vertically over 360 m (+330 to - 33 m) on fifteen levels (Lavrič and Spangenberg, 2003). Ore minerals are cinnabar, metacinnabar, native mercury, pyrite and scarce barite (Palinkaš et al., 2008). The host rocks and ore itself contain organic matter as disseminated kerogen, black solid hydrothermal bitumen, and greenish idrialite, a complex mixture of polycyclic aromatic hydrocarbons containing nitrogen and sulfur-bearing compounds (Lavrič and Spangenberg, 2001). Half a millennium of Hg production has resulted in elevated mercury content in all environmental compartments (Gosar et al., 2016). The Soca River (Isonzo River in Italy) and its tributary, the Idrija River, have drained for centuries the Hg-enriched deposits of the Idrija mine, resulting in trapping of Hg in the sediments of the Gulf of Trieste, that in turn constitute a net source of MeHg (Faganeli et al., 2003). On the banks of the Idrija River, the total Hg and MeHg concentrations in soils are ranging from 0.25 to 1650 mg/kg and not detected to 0.44 mg/kg, respectively (Tomiyasu et al., 2017). Hg levels in foodstuffs from the Idrija mine area were higher compared to those in food from non-contaminated areas (Miklavčič et al., 2013). Retired Idrija mine workers and Idrija residents occupationally unexposed contained much higher Hg concentrations in their tissues (sampled by autopsy) than control individuals (Falnoga et al., 2000). It was shown that the long-term occupational exposure to Hg endured by the Idrija mine workers caused renal dysfunction (Franko et al., 2005). In 2012, Almadén and Idrija were included to the Mercury World Heritage list of the UNESCO. Total Hg concentration in contaminated soils has been reported to vary between 8.4 and 415 mg/kg (Kocman et al., 2004) and between 0.3 and 973 mg/kg (Gosar et al., 2006).

Hg reduces the diversity of bacterial communities in soil, and this decrease is directly proportional to the Hg concentration in soil (Rasmussen et al., 2000). To survive such a hostile environment bacteria are endowed with the *mer* operon. This operon provides bacterial resistance to inorganic and organic Hg through the action of the mercuric reductase encoding *mer*A gene and the organomercurial lyase encoding *mer*B gene (Barkay et al., 2003; Mathema et al., 2011). Genes of the *mer* operon (*mer*A and *mer*B) have been previously detected in water samples downstream of the mine, not upstream (Hines et al., 2000). The Hg-resistant bacterium *Acinetobacter idrijaensis* has been isolated from a soil on the Idrija site. It contains in its genome the *merB, merA, merP, merT,* and *merR* genes (Campos-Guillén et al., 2014). This strain is able to grow in the presence of high concentrations of $HgCl_2$ (200 mg/L, 737 μM) and catalyzes the volatilization of Hg (*merA* gene).

Here, we document a new bacterial species named *Pseudomonas idrijaensis.* It has been recovered from a rock of the Idrija mine situated approximately 104 m below the surface and containing as much as 2952 mg Hg/kg. We show that this bacterial strain can thrive in such a toxic environment because it contains the *mer* operon in its genome. Another goal of the present study was to address the question related to the chemical forms of the Hg atoms within the bacterial cells after exposure to inorganic Hg and the possible influence of the *mer* operon on these chemical forms.

2. Materials and methods

2.1. Sampling and characterization of the rock

A piece of black shale/siltstone from the Upper Ladinian formation was sampled aseptically in April 2017 at the third mine level, 110 m below the entrance to Borba Shaft situated 226 m above sea level (Fig. S1). The rock was put in a sterile glass bottle and transferred to the laboratory within 4 h. We chose this rock because it contained both native elemental mercury and organic matter. The air temperature in mine was 13 °C and the air humidity 84% at the time of sampling.

The chemical composition of the bulk sample was determined by the ACME Analytical Laboratory, Canada. Major oxides were determined by ICP-MS after fusion in lithium borate and digestion in dilute nitric acid (Table 1). Aqua Regia digestion and ICP-ES/ICP-MS analysis were used for selected elements (As to Zn in Table 2). Carbon and sulfur were determined using a LECO analyzer. The mineral composition was determined by X-ray powder diffraction (XRD) using a Philips diffractometer (graphite monochromator, CuKα radiation, proportional counter). The mineral phases were identified using the Powder Diffraction File (1996) data system and the Panalytical XPert HighScore (v. 1.0d) program package. Phyllosilicates were identified using published methods (Moore and Reynolds, 1989). Semi-quantitative estimates of minerals were obtained from measurements of the relative peak intensities. Relative abundances are presented with Xs (Table S1). The pH value of the rock sample was determined after dispersion of its powder (1:2.5) in distilled water.

2.2. Isolation and characterization of *Pseudomonas idrijaensis*

Ten grams of rock from the Idrija mine were crushed in a mortar

Table 1
Chemical composition (in wt. %) of the rock.

SiO_2	Al_2O_3	Fe_2O_3	MgO	CaO	Na_2O	K_2O	TiO_2	P_2O_5	LOI[a]	Sum
56.94	15.41	4.13	1.36	4.96	0.50	2.78	0.62	0.15	12.9	99.75

[a] Loss on ignition (1000 °C).

Table 2
Content of sulfur, carbon and selected trace elements in the rock. [a]

S	C	As	Ba	Bi	Cd	Co	Cu	Hg	Mo	Ni	Pb	Sb	U	V	Zn
2.61	1.91	24.6	258	3.1	<0.1	9.9	23.3	2952.0	11.3	9.8	21.1	15.7	11.2	118	41

[a] S and C in wt. %, As to Zn in mg/kg.

and the powder suspended in peptone water. The suspension was concentrated on sterile membrane filters with 0.45 μm pore size and placed on Nutrient Agar (Biolife). Plates were incubated aerobically at 22 °C for 72 h, after which the growth of colonies was checked. Only one morphological type of colony was grown. It was recultivated in pure culture. The isolate was characterized initially by routine bacteriological techniques.

Before whole genome sequencing the isolated bacterium was identified by matrix-assisted laser desorption ionization-time of flight mass spectrometry - MALDI-TOF MS, as described in the Supporting Information (SI, paragraph 1).

2.3. Determination of mercury chloride minimum inhibitory concentration (MIC) and resistance tests

The MICs values to mercury chloride exposure were determined for the *P. idrijaensis* and *P. aeruginosa* PAO1 strains. The PAO1 strain is a reference strain known to be sensitive to mercury. Bacterial cultures were grown overnight in Luria-Bertani (LB) medium and diluted to an OD_{600} of 0.01. Then 2 ml of the diluted overnight culture were dispensed in 10 ml plastic tubes containing 50 μl of a blend made up with water and a stock solution of $HgCl_2$ in order to reach final concentrations between 0 and 100 μM $HgCl_2$. The stock solution of $HgCl_2$ was prepared at a concentration of 20 mM (4 g/L). Each final concentration was assayed in triplicate for each bacterial species. After 16 h of incubation at 37 °C, cell growth was monitored by spectrometry (absorbance at 600 nm) and MICs values were registered.

Resistance tests to $HgCl_2$ and monomethylmercury chloride (MeHgCl) were carried out at the surface of agar-containing LB medium. 50 μl bacterial cultures in overnight LB medium were spread over plastic Petri dishes containing 15 ml agar-jellified LB medium. 15, 30, 150, and 300 μg of Hg from 4 to 40 g/L $HgCl_2$ and from 5 to 50 g/L MeHgCl stock solutions were spiked at the center of the Petri dishes and the boxes incubated at 37 °C for 20 h. The same assay was repeated at 15 °C for 48 h. The growth inhibition was read as the diameter of the zone of inhibition.

2.4. Genomic DNA extraction

From a fresh streak of *P. idrijaensis* on an agar-jellified LB medium, 6 ml of liquid LB medium were inoculated and grown overnight at 37 °C. The bacterial genomic extraction followed a published recipe (Wilson, 2001). Briefly, the bacteria were lysed with SDS and proteinase K, and the genomic DNA treated with CTAB/NaCl, then extracted with chloroform/isoamylic alcohol (24:1) and afterward with phenol/chloroform/isoamylic alcohol (25:24:1). The genomic DNA was precipitated with 0.6 volume of isopropanol, and after centrifugation washed with 70% ethanol, then dried. The genomic DNA was dissolved in 10 mM Tris, 1 mM EDTA (TE buffer pH 8.0). After quantification of its concentration by UV spectrometry at 260 nm (Nascimento and Chartone-Souza, 2003 apparatus, Thermo Fisher Scientific), the genomic DNA was diluted in TE to a concentration of 0.1 mg/mL.

2.5. Whole genome sequencing

The *P. idrijaensis* genome has been sequenced by the Genome Scan company (Leiden, The Netherlands) using Illumina next generation sequencing technology (Illumina Hiseq 4000). Data were assembled with Spades v3.11.1.

2.6. Exposure to $HgCl_2$ for XANES spectroscopy

From a fresh streak of *P. idrijaensis* on an agar-jellified LB medium, 3 ml of liquid LB medium were inoculated and grown overnight at 37 °C. Then 50 ml of LB were inoculated with that culture and grown at 37 °C for 8 h. With this starting culture, 2 L of LB were inoculated and grown overnight at 37 °C. The resulting turbidity was 0.96 at 600 nm, corresponding to 0.288 g biomass (one unit of OD_{600} corresponds to 0.3 g/L bacteria). The 2 L culture was split in two 1 L bottles and centrifuged for 10 min at 5000 rpm in a JLA8.1 rotor (Beckman-Coulter Avanti JXN-26 centrifuge). Each cell centrifugate was washed with 250 ml of sterile minimally complexing medium (MCM buffer). The composition of the MCM buffer was slightly modified from Dahl et al. (2011): 20 mM 3-(N-morpholino) propane sulfonic acid (MOPS buffer), 0.41 mM $MgCl_2$, 6 mM $(NH_4)_2SO_4$, and 10 mM glucose. Each cell pellet was resuspended in 500 ml of MCM and spiked with $HgCl_2$ from a 20 mg/L $HgCl_2$ stock solution. 100 μl were added to one cell batch and 1 ml to the other batch yielding nominal concentrations of 4 and 40 μg Hg/L, respectively (19.9 and 199 nM). The two cultures were incubated at 37 °C for 195 min, then each culture was split in two and centrifuged for 10 min at 5000 rpm in a JLA8.1 rotor. Two cell pellets (one exposed to 4 and the other to 40 μg Hg/L) from split 1 were used to analyze mercury speciation in whole bacterial cells (Tot fraction). These cell pellets were washed with 45 ml of MCM and centrifuged in 50 ml Falcon tubes at 4500 rpm for 10 min (in swinging buckets n° 8172, using the centrifuge Heraeus Labofuge 400R, Thermo Scientific). The two remaining other cell pellets (one exposed to 4 and the other to 40 μg Hg/L) were used to analyze mercury speciation in the intracellular bacterial compartment (Intra fraction). To remove mercury from the cell membrane and cell wall without compromising the cytoplasmic membrane integrity, a two-step washing procedure was used (Thomas and Gaillard, 2017). Cell pellets were resuspended in 200 mL of 50 mM EDTA and 100 mM oxalate solution (pH = 7.5) and after 10 min of reaction were centrifuged for 10 min at 5000 rpm in a JLA8.1 rotor. The centrifugates were resuspended in 50 mL of a 10 mM reduced glutathione and 3 mM ascorbate solution (pH = 7). After 5 min of reaction, the suspensions were centrifuged in 50 ml Falcon tubes at 4500 rpm for 10 min, and the cells washed with 45 ml MCM then centrifuged in 50 ml Falcon tubes at 4500 rpm for 10 min. The four cell preparations were lyophilized after 1 h of storage at −80 °C. The four final bacterial biomasses weighed about 250 mg.

2.7. Measure of Hg concentration

Mercury in the four preparations was quantified with a DMA-80 mercury analyzer (Milestone Dual-cell). The detection limit was 0.003 ng Hg and accuracy was confirmed by analysis of the IAEA-436 reference from the International Atomic Energy Agency. The

recommended value is 4.19 $\pm$ 0.36 mg kg^{-1} d. w. and the determined value was 3.98 $\pm$ 0.13 mg Hg kg^{-1} dry weight ($n = 21$).

2.8. XANES identification of the mercury species in P. idrijaensis exposed to HgCl$_2$

Mercury L3-edge high energy-resolution XANES (HR-XANES) spectra were measured at 10−15 K with high-reflectivity analyzer crystals (Rovezzi et al., 2017) on beamline ID26 at the European Synchrotron Radiation Facility (ESRF). Data were analyzed against a large database of spectra for mercury minerals (α-HgS, β-HgS, β-HgS$_{NP}$), Hg(II) complexes in natural organic matter, and Hg(II) and methylmercury (MeHg) model complexes with thiolate ligands (Manceau et al., 2015a, 2015b; 2016, 2018; 2019; Bourdineaud et al., 2019). All reference spectra were considered as a basis for identification, but only diagnostic spectra are discussed herein.

The proportions of the Hg species were evaluated using least-squares fitting (LSF) of the experimental spectra with linear combinations of the component spectra. The regression analysis was performed by minimizing the normalized sum-squared residual $NSS = \Sigma[(y_{exp}\text{-}y_{fit})^2]/\Sigma(y_{exp}^2)$. The precision of the percentage of a fit component was estimated to be equal to the variation of its optimal value when the fit was degraded by 20% (i.e., 20% increase of NSS).

3. Results

3.1. Characterization of the rock

The pH value of the rock powder was 3.67. Quartz and mica are the main constituents (Table S1), in agreement with chemical analysis (Tables 1 and 2). They are followed by kaolinite and gypsum. Pyrite, goethite and rozenite are minor (Table S1). Goethite, rozenite and gypsum are weathering products of pyrite. No mercury-bearing phases such as cinnabar and metacinnabar were identified in the sample. Yet, this rock contains a high level of mercury, 2952 mg/kg, and several other toxic metals and metalloids at a concentration above 10 mg/kg: As, Mo, Pb, Sb, U, and V (Table 2).

3.2. Characterization of P. idrijaensis

The bacterial isolate recovered from the rock possesses the following characteristics: Gram-negative rod, oxidase and catalase positive, no reaction on the Kligler Iron Agar. The MALDI-TOF MS identification yielded 10 consecutive score values form 1.198 to 1.462 for *Pseudomonas* spp (Table S2). The findings indicate reliable identification of the genus *Pseudomonas*, but unsuccessful species identification. The isolate proved to be sensitive to all tested antibiotics (Table 3).

Over the course of the search for the *mer* operon genes and

Table 4
Compared sensitivity of *P. idrijaensis* to inorganic and organic mercury.

Quantity of mercury (μg) [a]	Growth inhibition zone diameter (mm)		Ratio [b]
	P. aeruginosa PAO1	*P. idrijaensis*	
HgCl$_2$			
15	20 $\pm$ 1	8 $\pm$ 1 [c]	6.2
30	23 $\pm$ 1	11.5 $\pm$ 1.5 [c]	4.0
150	33 $\pm$ 2	17 $\pm$ 1 [c]	3.8
300	40 $\pm$ 2	22 $\pm$ 1 [c]	3.3
MeHgCl			
15	23 $\pm$ 2	26 $\pm$ 1	0.8
30	28 $\pm$ 1	32 $\pm$ 4	0.8
150	46 $\pm$ 2	48 $\pm$ 2	0.9
300	59 $\pm$ 1	55 $\pm$ 3	1.1

[a] solution containing the indicated quantity of mercury was laid at the center of the Petri dish.
[b] Ratio of surfaces of growth inhibition between PAO1 and *P. idrijaensis*.
[c] Asterisks indicate significant differences between PAO1 and *P. idrijaensis* growth inhibitions ($P < 0.05$, $n = 3$).

before processing to the whole genome sequencing, a 2278 bp fragment was amplified using the R1 and A5 primers targeting the *mer*R and *mer*A genes, respectively (SI, paragraph 2). After cloning and sequencing, this fragment appeared to be unrelated to the *mer* operon because the R1 probe had hybridized to both extremities of the amplified fragment. The closest sequence retrieved from a blast inquiry of GenBank was that of the formate dehydrogenase α subunit of *Pseudomonas alkylphenolica*, strain KL28 (GenBank accession number CP009048) (Mulet et al., 2015). The two DNA sequences were identical at 94%. After whole genome sequencing the *P. idrijaensis fdo*G2 gene proved to determine the synthesis of an 808 residues protein best matching with its *P. alkylphenolica* counterpart with a 97.6% identity. These genetic data confirm the mass spectrometry identification of *Pseudomonas* spp. Due to highly repetitive sequences, part of the *P. idrijaensis* genome could not be sequenced and that part included the 16S rRNA genes. Therefore, the classical identification through 16S rRNA sequence comparisons could not be performed.

3.3. Resistance of P. idrijaensis to mercury chloride and sensitivity to methylmercury chloride

After 16 h of incubation in liquid LB medium at 37 °C, the highest concentrations of HgCl$_2$ for which no impact on cell growth was observed were 5 μM for *P. aeruginosa* PAO1 and 80 μM for *P. idrijaensis*. The MICs of HgCl$_2$ were 10 μM for PAO1 and 90 μM for *P. idrijaensis*. The growth surfaces were three-to six-times less inhibited than those of PAO1 depending on the amount of Hg(II) (Table 4). Thus, *P. idrijaensis* is clearly resistant to Hg(II). However,

Table 3
MIC and zone diameter values of antibiotics against environmental isolate of *P. idrijaensis*.

Antimicrobial category	Antibiotic	MIC (mg/L)	Zone diameter (mm)[a]
carbapenems	MEM - meropenem	1	27
	IMI - imipenem	1	32
fluoroquinolones	CIP - ciprofloxacin	$\leq$0.25	30
aminoglycosides	GEN - gentamicin	$\leq$1	28
	AMK - amikacin	$\leq$2	30
	NET - netilmicin		27
cephalosporins	CAZ - ceftazidime	$\leq$1	18
	FEP - cefepime	$\leq$1	30
penicillins	TZP - piperacillin/tazobactam	8	26
polymyxins	CST - colistin	$\leq$0.5	0.75

[a] Determined by E-test. Isolate was sensitive to all tested antibiotics according to EUCAST criteria.

the two strains featured the same sensitivity to methylmercury chloride (Table 4). Results were independent of the temperature of growth (37 and 15 °C).

3.4. Identification of the mer operon genes in P. idrijaensis

The resistance tests suggested that the *P. idrijaensis* strain harbored at least the *mer*R, *mer*P, *mer*T and *mer*A genes encoding the mercuric reductase in response to Hg(II) exposure, whereas *mer*B encoding the organomercurial lyase was absent. Before processing to the whole genome sequencing we first obtained PCR evidences of the presence of the *mer* operon within the bacterium's genome (SI, paragraph 3 and Fig. S2). The amplified fragments revealed that the organization of the *mer* operon was RTPCA, with *mer*R transcribed in opposite direction relative to *mer*TPCA (Fig. S2).

The whole genome sequencing of *P. idrijaensis* confirmed the existence of a *mer* operon with the genes organization deduced

from PCR analysis. However, it also contains the *mer*D and *mer*E genes (Fig. 1). The *mer* operon is contained within the Tn*5041* transposon. A blast of scaffold 5 from *P. idrijaensis* matched the Tn*5041* sequence from a *Pseudomonas* species isolated from the soil of the Khaidarkan mercury mine, Kirghizia, Central Asia (Kholodii et al., 1997). Out of 14,907 nucleotides composing the transposon, only 7 did not co-occur in the two *Pseudomonas* species. Their locations in the Tn*5041*sequence are shown with asterisks in Fig. 1, along with some remarkable genomic characteristics of this sequence. The extended organization of the *mer* operon is RTPCAYDE with an open reading frame *orf*Y intercalated between the *mer*A and *mer*D genes. The function of the hypothetical protein encoded by *orf*Y is unknown. The transcriptional regulatory signals involved in the *mer* genes expression are present and intact. They lie within the intergenic region between *mer*R and *mer*T. There is a potential binding site for MerR repressor, <u>ccgta</u>catgact<u>acgg,</u> with its inverted repeats (underlined), and there are − 35 and − 10 signals
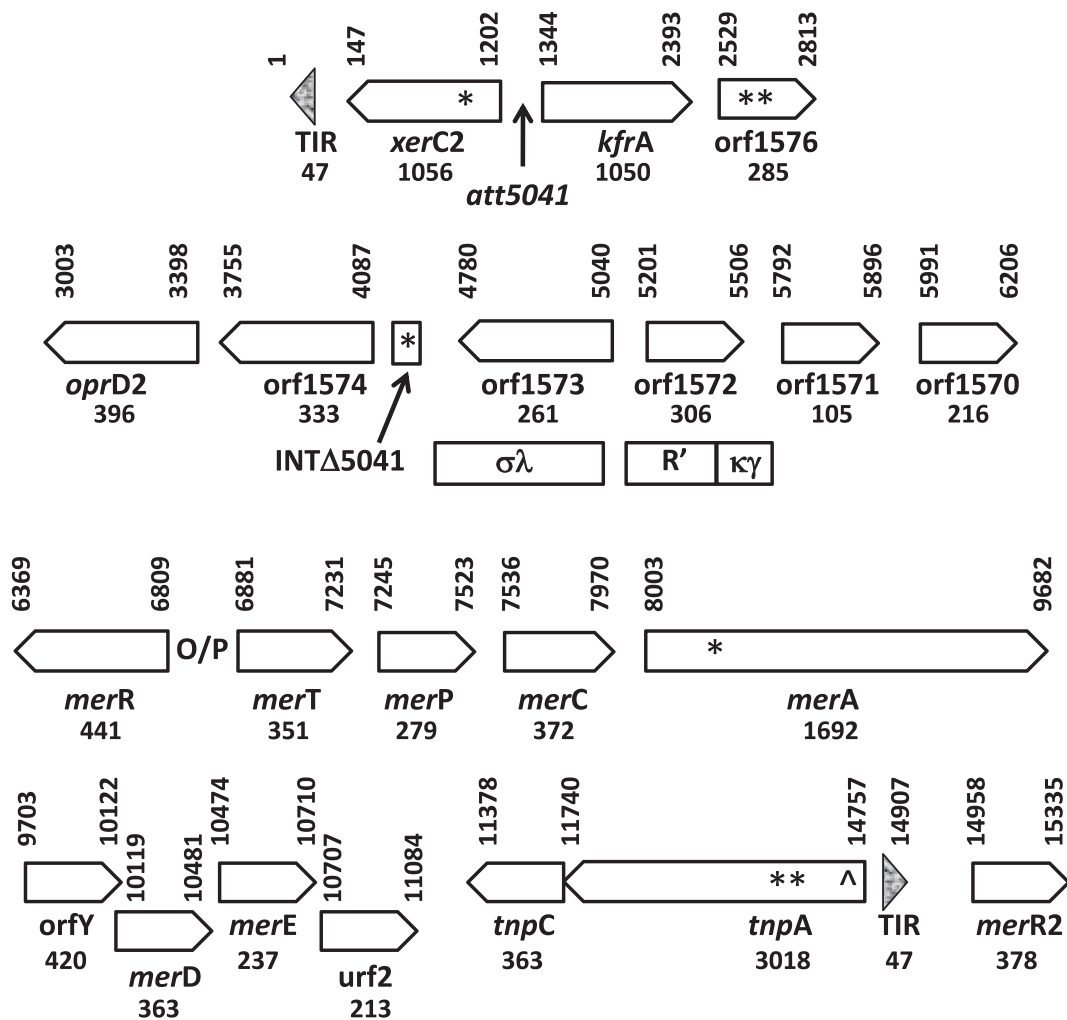

Fig. 1. Organization of the *mer* operon of *P. idrijaensis* inside the Tn*5041A* transposon. The numbers above the arrows symbolizing the Tn*5041* elements indicate the positions of the genes and open reading frames (orf, putative genes coding for hypothetical proteins), and some remarkable genetic elements in the 14,907 bp-long transposon. The numbers below the arrows indicate the length in bp of the genetic elements. Arrows point in direction of the transcription. XerC2 is an integrase; KfrA is a DNA binding protein involved in the transposition process; OprD2 is an outer membrane porine; TnpC is a repressor of the *tnpA* gene; TnpA is a transposase of the Tn3-family transposon. The two uncoding TIR sequences are terminal inverted repeats that flank the transposon on its extremities. *att5041* is the attachment site. INTΔ5041 is a 195 bp-long truncated group II intron. R′ is a truncated copy of *merR*. σλ and κγ are relics of mobile elements: σλ is a defective element showing some homology with the insertion sequences IS2 and ISRm1, and κγ is a defective minitransposon of the Tn3-family with terminal inverted repeats. The σλ, R′ and κγ elements overlap with orfs 15,723 and 1573. The regulatory *cis* elements O/P are the promoter and operator of the *mer* operon. The locations of the 7 nucleotides distinguishing Tn*5041A* of *P. idrijaensis* and *Pseudomonas* sp. from the Khaidarkan mine are indicated with asterisks. The substitutions are 811: A/G (A in *P. idrijaensis* and G in the Khaidarkan bacterium); 2557: T/A; 2558: T/A; 4252: C/T; 8346: C/T; 13,835: A/T; 13,836: A/T. The symbol ^ indicates the location of the single nucleotide distinguishing Tn*5041A* of *P. idrijaensis* and both *P. putida* DRA525 and *Pseudomonas* sp. strain 1239. It is located at position 14,729: G/C (*P. idrijaensis*/DRA525).

allowing transcription of *mer*TPCAYDE in one direction and those for the *mer*R gene transcription in the opposite direction. Noteworthy is the existence of a second *mer*R gene, called *mer*R2, located 51 nucleotides downstream from the right arm of the Tn*5041* transposon materialized by the terminal inverted repeat (TIR) (Fig. 1). The encoded protein is 90% identical to a MerR family of transcriptional regulators contained in the genome of *Pseudomonas* sp. ERMR1:2, a strain isolated in India, East Rathong glacier, West Sikkim (protein accession number: PAM82489; nucleotidic accession number: NKJI01000010). The MerR2 protein contains only one cysteine residue versus 4 for the genuine MerR regulator. The function of MerR2 as a metal regulator has not been proven yet.

3.5. Mercury speciation after exposure to mercury chloride

The dry weight Hg concentrations of the bacterial masses analyzed by HR-XANES were [Pi-4-Tot] = 6.7 ± 0.2 μg Hg/g and [Pi-4-Intra] = 4.3 ± 0.2 μg Hg/g for the total and intracellular preparations exposed to 4 μg Hg/g, and [Pi-40-Tot] = 61 ± 1 μg Hg/g and [Pi-40-Intra] = 42 ± 4 μg Hg/g for those exposed to 40 μg Hg/g. The four HR-XANES spectra feature a near-edge peak at 12279.3 eV (indicator region "A" in Fig. 2a) characteristic of linear dithiolate complex (Hg(SR)$_2$) (Manceau et al., 2019). The straighter the RS-Hg-SR angle, the sharper is this peak. The trailing spectral edge of Pi-4-

Intra is shifted to lower energy in the 12,320−12340 eV interval (indicator region "B"). The shift is indicative of longer Hg−S bond distance and means that higher coordination complex, such as Hg(SR)$_3$ and Hg(SR)$_4$, coexists with the main Hg(SR)$_2$ complex (Fig. 2b). This Hg coordination effect, described previously with a comparison of the Hg(Cys)$_2$, Hg (D-penicillamin)$_3$, and Hg(Cys)$_4$ HR-XANES spectra (Manceau et al., 2019), is explained physically by the Natoli rule (Bianconi et al., 1983). The distinctive difference of Pi-4-Intra is better seen in its comparison with Pi-4-Tot (Fig. 2c). The shift in energy observed in region B is accompanied by a decrease in intensity of the near-edge peak in region A. This is because the RS-Hg-SR angles of the three-coordinate or four-coordinate complexes present in Pi-4-Intra and detected in region B are not linear (Fig. 2b). The coordination structures of Hg in Pi-4-Tot and Pi-4-Intra are examined in more detail below.

In Pi-4-Tot, Hg(II) is coordinated linearly to two thiolate ligands (Fig. 2c). The RS-Hg-SR bond axis from a Hg(SR)$_2$ complex is perfectly straight only when the Hg coordination is strictly two. The proximity to Hg atoms of oxygen and nitrogen donors from typically carbonyl and amine groups bends the RS-Hg-SR angle (Fig. 3a). On the HR-XANES spectra, this is reflected phenomenologically in a decrease of the near-edge peak intensity or sharpness, similarly to the bonding of a third (Hg(SR)$_3$) and fourth (Hg(SR)$_4$) thiol, but the effect here is more subtle because oxygen and nitrogen are weaker
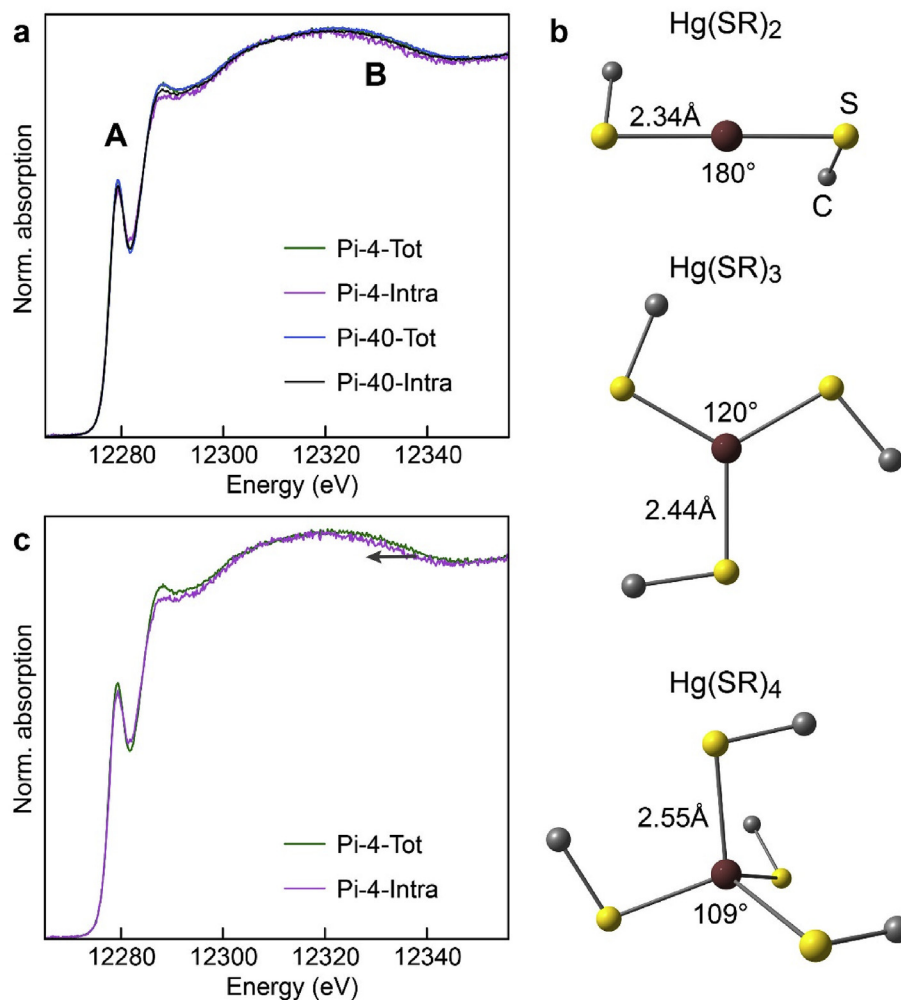

Fig. 2. HR-XANES spectra of *P. idrijaensis* cultures exposed to 4 μg (Pi-4) and 40 μg (Pi-40) Hg/L (a,c), and ball-and-stick representation of the Hg(SR)$_2$, Hg(SR)$_3$ and Hg(SR)$_4$ complexes (b). The Hg−S distances are from Manceau and Nagy (2008).
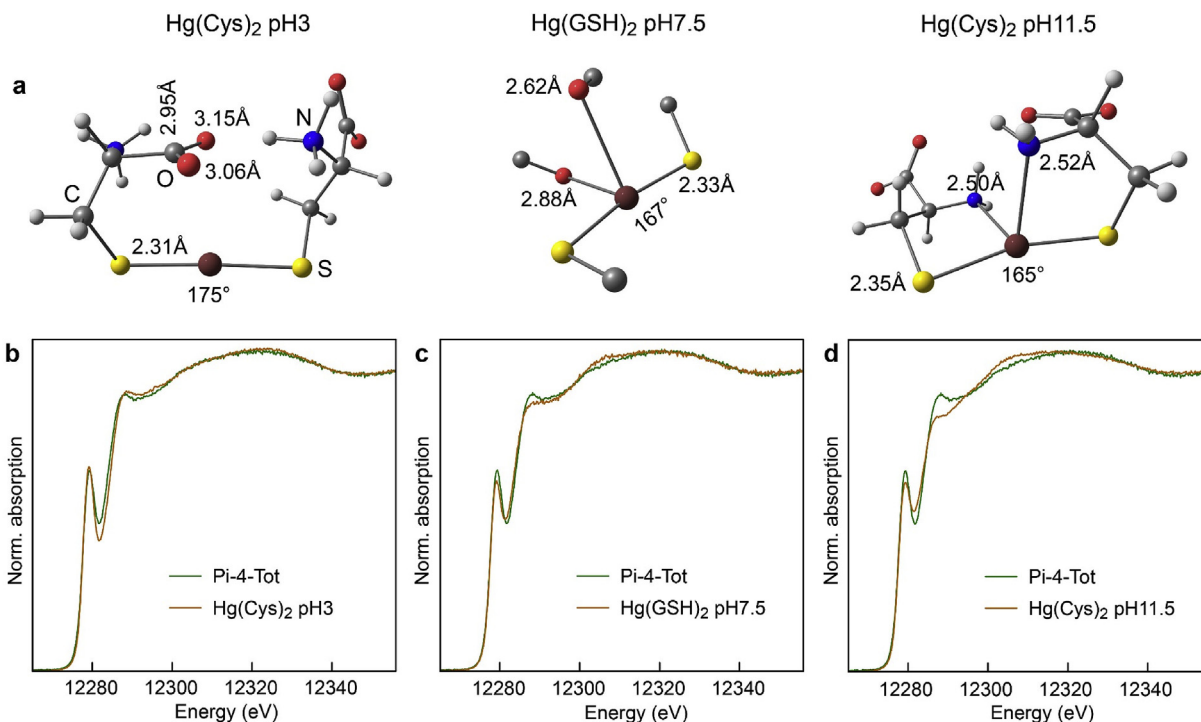
Fig. 3. Ball-and-stick representation (a) and HR-XANES spectra (b–d) of three dithiolate complexes differing in the second coordination shell compared to the spectrum of *P. idrijaensis* exposed to 4 μg Hg/L (Pi-4-Tot fraction). The ball-and-stick models are from Bourdineaud et al. (2019). Only the bonding environment of Hg is represented for Hg (glutathione)$_2$.

ligands. Moreover, the attenuation of the near edge peak occurs without modification of region B because the variation of the RS-Hg-SR angle caused by O/N donors does not change the Hg—S distance, in contrast to the addition of a third (Hg(SR)$_3$) and fourth (Hg(SR)$_4$) sulfur ligand (Fig. 2b). The effect of secondary Hg ….O/N interactions on HR-XANES is illustrated in Fig. 3b–d with the Hg [SR]$_2$, the Hg [SR + O]$_2$, and the Hg [SR + N]$_2$ coordinations from the Hg(Cys)$_2$ pH 3, Hg (GSH)$_2$ pH 7.5, and Hg(Cys)$_2$ pH 11.5 references (Bourdineaud et al., 2019). Pi-4-Tot has a near-edge intensity intermediate between those of the Hg [SR]$_2$ and the Hg [SR + O/N]$_2$ coordinations, which suggests that Hg is secondarily bonded to one O or N ligand on average. This bonding environment is a signature for biologic matter for it is not detected in natural organic matter (Manceau et al., 2015a).

Regarding Pi-4-Intra, the shift in energy of region B (Fig. 2c) has been observed previously in fish exposed to Hg(II)-doped dissolved organic matter (DOM) (Fig. 2a) (Bourdineaud et al., 2019): 84 ± 8% of the Hg in fish is two-coordinate (Hg(SR)$_2$) and 16 ± 8% is four-coordinate (Hg(SR)$_4$). A linear fit of Pi-4-Tot and Hg(Cys)$_4$ to Pi-4-Intra shows that the tetrathiolate species amounts to 13 ± 6 at%, or $4.3 \times 0.13 = 0.6$ μg Hg/g, inside the bacteria (Fig. 4b). The bacterium and fish spectra differ, however, in region A, the Pi-4-Intra near-edge being more intense than the near-edge of the fish spectrum. This difference was examined further by measuring the spectra of *Escherichia coli* and *Bacillus subtilis* exposed to 4 μg Hg/L. The two spectra were statistically identical, therefore averaged to obtain one spectrum representing bacteria with no *mer* operon. This spectrum is also distinctive from Pi-4-Intra in region A (Fig. 4c). The Pi-4-Intra spectrum was best-fit as a linear combination of 43% of the *E. coli-B. subtilis* spectrum plus 56% of the Hg(Cys)$_2$ spectrum (±6 at%) (Fig. 4d). Thus, higher amounts of the mercury dithiolate species distinguishe *P. idrijaensis* equipped with the *mer* operon. The two Hg(SR)$_3$ references from our database (Manceau et al., 2019) were both unsuitable models.

4. Discussion

The rock sample contains four times less Hg (2952 mg/kg) than the Idrija deposit on average (Mlakar, 1974), and almost seventeen times less than the Almadén mine on average (5%, Higueras et al., 2011). The Hg content of 2952 mg/kg is, however, two times higher than the highest Hg content of 1650 mg/kg reported in soil near the Idrija mine (Tomiyasu et al., 2017).

Comparison of the amounts of Hg added to the living bacteria and measured in the biomass after 195 min exposure shows that bacteria took up almost all the added Hg and volatilized little Hg. In the 40 μg Hg/L experiment, 0.288 g biomass was exposed to 20 μg Hg(II) in 500 ml giving an initial Hg concentration equal to 69 μg Hg/g bacteria dw. The initial Hg concentration was 6.9 μg Hg/g bacteria dw in the 4 μg Hg/L experiment. At the end of the experiment, [Pi-40-Tot] = 61 ± 1 μg Hg/g dw and [Pi-4-Tot] = 6.7 ± 0.2 μg Hg/g dw. Thus, bacteria sorbed and retained 89% and 97% of total Hg in the exposure medium. Furthermore, comparison of total and intracellular Hg concentrations shows that two thirds of the Hg diffused into the bacterial cell. Thus, *P. idrijaensis* efficiently uptakes Hg. 10^{12} dry bacteria weigh 0.3 g, corresponding to 3.33×10^{12} bacteria/g dw. After exposure to 40 μg Hg/L, 42 μg Hg/g inside the cells represent $(42 \times 10^{-6} \text{ x } 6 \times 10^{23})/(200.6 \times 3.33 \times 10^{12}) = 37.8 \times 10^3$ atoms of Hg/bacterial cell. In turn, knowing the volume of a bacterial cell, 1.67 μm^3 during the exponential phase of growth in a rich medium (Kubitschek and Friske, 1986), we can calculate an internal Hg concentration of $(37.8 \times 10^3)/(6 \times 10^{23} \text{ x } 1.67 \times 10^{-15}) = 37.7$ μM, resulting in a bioaccumulation factor of 189. After exposure to 4 μg Hg/L, 4.3 μg Hg/g inside the cells represent 3.9×10^3 atoms of Hg/bacterial cell, making 3.9 μM Hg, therefore a bioaccumulation factor of 196. Such high bioaccumulation factors likely result from the intervening action of the three transporters MerC, MerE and MerT.

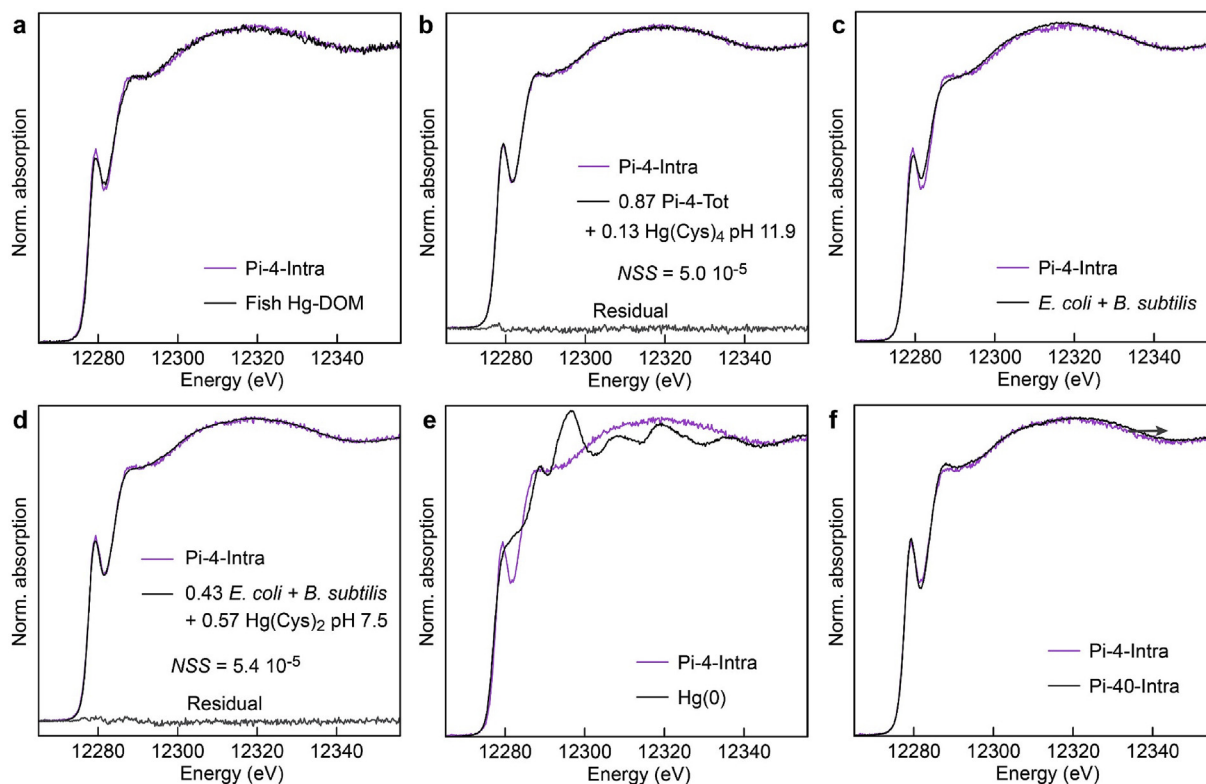A sharper near-edge peak of the HR-XANES spectrum

Fig. 4. Comparison of the HR-XANES spectrum from the intracellular fraction of *P. idrijaensis* exposed to 4 µg Hg/L (Pi-4-Intra) with the spectrum from fish exposed to Hg-doped DOM (a), with the average spectrum of the intracellular fractions of *E. coli* and *B. subtilis* exposed to 4 µg Hg/L (c), and with elemental Hg (e). Linear least-squares fit to the Pi-4-Intra spectrum with $87 \pm 6\%$ Pi-4-Tot and $13 \pm 6\%$ Hg(Cys)$_4$ at pH 11.9 (b), and with $43 \pm 6\%$ *E. coli* + *B. subtilis* and $57 \pm 6\%$ Hg(Cys)$_2$ at pH 7.5 (d). Comparison of the Pi-4-Intra spectrum with the intracellular spectrum from *P. idrijaensis* exposed to 40 µg Hg/L (Pi-40-Intra) (f).

distinguishes *P. idrijaensis* equipped with the *mer* operon. This feature indicates a higher content of the linear coordination of the Hg atom. The three-coordinate Hg-MerR complex induces expression of genes encoding for a series of membrane-bound proteins (MerT, MerC, MerE, MerF, MerH) and the periplasmic protein MerP, which coordinate Hg(II) linearly (MerT, MerC, MerF, MerP; Nascimento and Chartone-Souza, 2003; Serre et al., 2004; Silver and Hobman, 2007; Steele and Opella, 1997; Wilson et al., 2000; Sahlman et al., 1997), or are assumed to do so (MerE and MerH; Kiyono et al., 2009; Schué et al., 2009). Therefore, the enhanced near-edge structure of *P. idrijaensis*, explained by a richer content in Hg dithiolate complex, is probably a signature for the *mer* operon. Consistent with this hypothesis, the least-squares fitting of Pi-4-Intra with the *E. coli* + *B. subtilis* reference spectrum suggests that 57% of the Hg is bound to a dicysteine Mer protein (Fig. 4d). This molecular form of mercury, induced by the *mer* operon, could be viewed as a detoxification mechanism of its own.

Divalent mercury is reduced to gaseous Hg (0) by the action of the homodimeric mercuric reductase MerA (Fox and Walsch, 1982; Schiering et al., 1991; Hamlett et al., 1992). The coordination of Hg(II) in each monomer is two-coordinate, and its transfer to the catalytic active site occurs via a T-shape (SR$_{2+1}$) intermediate complex (Lian et al., 2014). Fig. 4e shows that Hg (0) has a distinct HR-XANES spectrum characterized by intense Hg−Hg oscillations in the top-edge region. This species is clearly absent in Pi-4-Intra.

The nature of the intracellular four-coordinate species is uncertain. The sulfur ligand can be thiolate, as in metalloprotein Hg(SR)$_4$ complex and in Hg$_x$(SR)$_y$ metallothionein cluster (Manceau et al., 2019), or inorganic sulfide, as in β-HgS (Thomas and Gaillard, 2017; Thomas et al., 2018; Manceau et al., 2018). The second hypothesis was tested by exposing *P. idrijaensis* to 10

times as much Hg (i.e., 40 µg Hg/L) as Pi-4-Intra to see if more β-HgS precipitated. The Pi-40-Intra spectrum has a trailing edge shifted to higher energy relative to Pi-4-Intra, which means less β-HgS, thus dismissing the β-HgS hypothesis (Fig. 4f). The four coordinate species may be linked to the bacterial metallothionein (MT) SmtA/BmtA. This MT, discovered in cyanobacteria, is also present in the *Pseudomonas* genus (Blindauer et al., 2002; Blindauer, 2011). The NMR structures give a Zn$_4$Cys$_9$His$_2$ cluster for *Synechococcus* SmtA (Blindauer et al., 2001), and Zn$_3$Cys$_9$His and Cd$_4$Cys$_9$His clusters for *P. fluorescens* PflQ2 (Habjanič et al., 2018). High similarities of structure were observed between the Zn$_4$SmtA and Cd$_4$PflQ2 clusters and the [Cd$_4$Cys$_{11}$] cluster of the α-domain in rat MT2 (Blindauer et al., 2001; Habjanič et al., 2018), and between the Zn$_3$PflQ2 cluster and the [Cd$_3$Cys$_9$] cluster of the β-domain in human MT2 (Habjanič et al., 2018).

The *mer* operon of *P. idrijaensis* is contained in the Tn*5041* transposon discovered in a *Pseudomonas* strain (KHP41) from the Khaidarkan mercury mine in Kirghizia (Kholodii et al., 1997). Tn*5041* most likely acquired the *mer* operon from a transposon belonging to the Tn*21* subfamily of the Tn*3* transposon family (Kholodii et al., 1997). *A. idrijaensis*, the other strain found in soil of the Idrija mine, does not possess the Tn*5041* element. This bacterium is endowed with two *mer* operons simply separated by the gene of a hypothetical protein and possessing only one *mer*R gene. The organization of the two *mer* operons is ED$_1$BR and D$_2$TPAG with the genes E, D1, B, D2 transcribed in one direction and the genes R, T, P, A, G transcribed in the opposite direction. Two *mer*D genes are present, and the relative MerD1 and MerD2 proteins display 61% of identity. The MerD protein from *P. idrijaensis* is 53% and 40% identical to *A. idrijaensis* MerD1 and MerD2, respectively.

The Tn*5041*-like elements can be divided in 12 types, based on

the genetic sequences isolated from several strains originating from mercury mines (Khaidarkan, Caucasus, Carpathians), Russian and American soils, and Russian rivers (Kholodii et al., 2002). Since the Tn*5041* transposons from *P. idrijaensis* and *Pseudomonas* KHP41 differ by only 7 nucleotides over 14,907, the new transposon identified here is assigned to the Tn*5041A* type like to the one from the reference strain KHP41. *P. putida* DRA525 isolated from an artisanal gold mining camp in Mozambique also harbors a Tn*5041*-hosted *mer* operon (Drace et al., 2018). It differs from the *P. idrijaensis* transposon by only one nucleotide and therefore also belongs to the Tn*5041A* type (indicated in Fig. 3). Hg-resistant bacteria endowed with Tn*5041* were not always isolated from soils or sediments polluted by mercury. This transposon has also been found in *Pseudomonas* bacteria isolated from Edoma suite sediments of the Siberian permafrost of Kolyma Lowland (late Pleistocene icy complex). The lowland is formed of fluvio-lacustrine loamy sediments aged from 15,000 to 40,000 years (Petrova et al., 2002; Mindlin et al., 2005). Some of the samples contained as little as 6−35 μg Hg/kg, therefore were uncontaminated. The Tn*5041* transposon of one permafrost strain (*P. fluorescens* ED23-70) has been sequenced. Compared with Tn*5041A* from KHP41, it contains two substituted nucleotides at positions 2875 and 3773, and has one additional short 47 nucleotides-long region (ρ) in the left arm at position 653−699 just after the putative attachment (*att*) site. This transposon was assigned to the B type Tn*5041B* (Mindlin et al., 2005). Recently, another Hg-resistant bacterium endowed with Tn*5041A*, the *Pseudomonas* sp. strain 1239, has been isolated from a soil sampled in the Loire valley, a location that is not affected by mercurial pollution (Crovadore et al., 2018). The sequence of the strain 1239 Tn*5041A* is identical to that of *P. putida* DRA525. In fact, the presence of the *mer* operon within a bacterial genome is not compulsory linked to a Hg-polluted environment: indeed, when seeking for bacteria sharing identical MerD, MerE and OrfY protein sequences with *P. idrijaensis*, the Blast search allowed retrieving 49 strains all belonging to the *Pseudomonas* genus. Among these 26 were clinical human isolates and 23 were environmental isolates. Among the latter, one had been isolated from a dairy product, 17 had been collected from sites unrelated to mercurial contamination, and only 5 had been sampled from Hg-polluted sites: one in the Khaidarkan mine (KHP41), one in a gold camp in Mozambique (DRA525), and 3 in the Oak Ridge Field Research Center (MPBC4-3, MPR-R5A and MPR-R5B) (Table S3).

Although the soil and rocks from the gold mining camp in Mozambique are devoid of antibiotics, as is also the case for those of the Idrija mine, *P. putida* DRA525 can resist to both Hg(II) and antibiotics. Resistance to antibiotics is conferred through the MexE-MexF-OprN multidrug efflux system (Drace et al., 2018). Co-resistance to both heavy metals enzymatically and antibiotics through efflux pumps is common (Baker-Austin et al., 2006) and probably explains why so many clinical isolates are also endowed with Hg resistance (Table S3). *P. idrijaensis* contains in its genome the MeA-MexB-OprM multidrug efflux system (one *mex*A gene, two *mex*B genes, and four *opr*M genes), which should confer broad-spectrum antibiotic resistance (Li et al., 2015). However, *P. idrijaensis* does not resist to known antibiotics, perhaps because it lacks the regulator gene *mex*R. The three genes *mex*A, *mex*B and *opr*M may not be expressed for they are not organized in an operon.

5. Conclusion

While the Tn*5041* element occurs most commonly on plasmids, it is inserted in the chromosome of *P. idrijaensis* like for the *Pseudomonas* strain KHP41, *Pseudomonas* sp. strain 1239 and *P. putida* DRA525 (Kholodii et al., 1997; Crovadore et al., 2018; Drace et al., 2018). This mobile element is old since it has been found in

P. fluorescens bacteria isolated from Siberian permafrost dated to the Pleistocene, about 15,000 to 40,000 BP (Petrova et al., 2002; Mindlin et al., 2005). The permafrost soil contained trace amounts of Hg like the Loire valley soil (from which has been isolated the strain 1239), which indicates that mercury contamination pressure is not compulsory to select this mercury resistance transposon once inserted in the chromosome. The presence of the *mer* operon proved to influence the mass distribution of the mercurial chemical species accumulated within bacterial cells after a challenge with inorganic Hg, with a relative enrichment in the dithiolate $Hg(SR)_2$ complex.

CRediT authorship contribution statement

Jean-Paul Bourdineaud: Conceptualization, Methodology, Validation, Investigation, Writing - original draft, Writing - review & editing, Visualization, Supervision, Project administration, Funding acquisition. **Goran Durn:** Methodology, Validation, Investigation, Writing - review & editing, Visualization. **Bojan Režun:** Resources. **Alain Manceau:** Methodology, Validation, Investigation, Writing - original draft, Writing - review & editing, Visualization, Funding acquisition. **Jasna Hrenović:** Conceptualization, Methodology, Validation, Investigation, Writing - review & editing, Visualization, Project administration, Funding acquisition.

Appendix A. Supplementary data

Supplementary data to this article can be found online at https://doi.org/10.1016/j.chemosphere.2020.126002.

References

Baker-Austin, C., et al., 2006. Coselection of antibiotic and metal resistance. Trends Microbiol. 14, 176−182.

Barkay, T., et al., 2003. Bacterial mercury resistance from atoms to ecosystems. FEMS Microbiol. Rev. 27 (2−3), 355−384.

Bianconi, A., et al., 1983. Bond length determination using XANES. In: Bianconi, A., Incoccia, A., Stipcich, S. (Eds.), EXAFS and Near Edge Structure. Springer Series in Chemical Physics, vol. 27. Springer-Verlag, Berlin, pp. 57−61.

Blindauer, C.A., et al., 2001. A metallothionein containing a zinc finger within a four-metal cluster protects a bacterium from zinc toxicity. Proc. Natl. Acad. Sci. U.S.A. 98 (17), 9593−9598.

Blindauer, C.A., et al., 2002. Multiple bacteria encode metallothioneins and SmtA-like zinc fingers. Mol. Microbiol. 45 (5), 1421-132.

Blindauer, C.A., 2011. Bacterial metallothioneins: past, present, and questions for the future. J. Biol. Inorg. Chem. 16 (7), 1011−1024.

Bourdineaud, J.-P., et al., 2019. Divalent mercury in dissolved organic matter is bioavailable to fish and accumulates as dithiolate and tetrathiolate complexes, 2019 Feb 5 Environ. Sci. Technol.. https://doi.org/10.1021/acs.est.8b06579

([Epub ahead of print]).

Brinck, J.W., van Wambeke, L., 1975. World Resources of Mercury. 1st Congr. Inter. del Mercurio, Barcelona, p. 39, 1974 (3/4).

Campos-Guillén, J., et al., 2014. Draft genome sequence of the mercury-resistant bacterium *Acinetobacter idrijaensis* strain MII, isolated from a mine-impacted area, Idrija, Slovenia. Genome Announc. 2 (6) e01177-14.

Crovadore, J., et al., 2018. Whole-genome sequence of *Pseudomonas putida* strain 1312, a potential biostimulant developed for agriculture. Microbiol Resour Announc 7 (10) e01097-18.

Dahl, A.L., et al., 2011. Bacterial bioreporter detects mercury in the presence of excess EDTA. Environ. Chem. 8, 552–560.

Drace, K., et al., 2018. Draft genome sequence of mercury-resistant *Pseudomonas putida* strain DRA525. Genome Announc. 6 (18) e00370-18.

Eucast, 2018. European Committee on Antimicrobial Susceptibility Testing. Break-point Tables for Interpretation of MICs and Zone Diameters. Version 8.0.

Faganeli, J., et al., 2003. Mercury and methylmercury in the Gulf of Trieste (northern adriatic sea). Sci. Total Environ. 304 (1–3), 315–326.

Falnoga, I., et al., 2000. Mercury, selenium, and cadmium in human autopsy samples from Idrija residents and mercury mine workers. Environ. Res. 84 (3), 211–218.

Fox, B., Walsh, C.T., 1982. Mercuric reductase. Purification and characterization of a transposon-encoded flavoprotein containing an oxidation-reduction-active disulfide. J. Biol. Chem. 257 (5), 2498–2503.

Franko, A., et al., 2005. Long-term effects of elemental mercury on renal function in miners of the Idrija Mercury Mine. Ann. Occup. Hyg. 49 (6), 521–527.

Gosar, M., et al., 2006. Binding of mercury in soils and attic dust in the Idrija mercury mine area (Slovenia). Sci. Total Environ. 369 (1–3), 150–162.

Gosar, M., et al., 2016. Distribution pattern of mercury in the Slovenian soil: geochemical mapping based on multiple geochemical datasets. J. Geochem. Explor. 167, 38–48.

Habjanič, J., et al., 2018. A histidine-rich *Pseudomonas* metallothionein with a disordered tail displays higher binding capacity for cadmium than zinc. Metall 10 (10), 1415–1429.

Hamlett, N.V., et al., 1992. Roles of the Tn*21 merT, merP*, and *merC* gene products in mercury resistance and mercury binding. J. Bacteriol. 174 (20), 6377–6385.

Higueras, P., et al., 2011. The Almadén mercury mining district. In: Ortiz, J.E., Puche, O., Rábano, I., Mazadiego, L.F. (Eds.), History of research in mineral resources. Cuadernos del Museo Geominero, n°13. Instituto geológico y minero de España, Madrid, pp. 75–88.

Hines, M.E., et al., 2000. Mercury biogeochemistry in the Idrija River, Slovenia, from above the mine into the Gulf of Trieste. Environ. Res. 83 (2), 129–139.

Kholodii, G.Y., et al., 1997. Tn*5041*: a chimeric mercury resistance transposon closely related to the toluene degradative transposon Tn*4651*. Microbiology 143 (8), 2549–2556.

Kholodii, G., et al., 2002. Tn*5041*-like transposons: molecular diversity, evolutionary relationships and distribution of distinct variants in environmental bacteria. Microbiology 148 (11), 3569–3582.

Kiyono, M., et al., 2009. The MerE protein encoded by transposon Tn*21* is a broad mercury transporter in *Escherichia coli*. FEBS Lett. 583 (7), 1127–1131.

Kocman, D., et al., 2004. Mercury fractionation in contaminated soils from the Idrija mercury mine region. J. Environ. Monit. 6 (8), 696–703.

Kubitschek, H.E., Friske, J.A., 1986. Determination of bacterial cell volume with the Coulter counter. J. Bacteriol. 168 (3), 1466–1467.

Lavrič, J.V., Spangenberg, J., 2001. Geochemistry of the Idrija mercury deposit, Slovenia: insight from δ^{13}C, δ^{18}O, δ^{34}S and organic geochemical data. In: Piestrzyński, et al. (Eds.), Mineral Deposits at the Beginning of the 21st Century. A.A. Balkema, Rotterdam, pp. 55–58.

Lavrič, J.V., Spangenberg, J., 2003. Stable isotope (C, O, S) systematics of the mercury mineralization at Idrija, Slovenia: constraints on fluid source and alteration processes. Miner. Deposita 38, 886–899.

Li, X.Z., et al., 2015. The challenge of efflux-mediated antibiotic resistance in Gram-negative bacteria. Clin. Microbiol. Rev. 28 (2), 337–418.

Lian, P., et al., 2014. X-ray structure of a Hg^{2+} complex of mercuric reductase (MerA) and quantum mechanical/molecular mechanical study of Hg^{2+} transfer between the C-terminal and buried catalytic site cysteine pairs. Biochemistry 53 (46), 7211–7222.

Manceau, A., Nagy, K.L., 2008. Relationships between Hg(II)-S bond distance and Hg(II) coordination in thiolates. Dalton Trans. 11, 1421–1425.

Manceau, A., et al., 2015a. Structure, bonding, and stability of mercury complexes with thiolate and thioether ligands from high-resolution XANES spectroscopy and first-principles calculations. Inorg. Chem. 54, 11776–11791.

Manceau, A., et al., 2015b. Formation of mercury sulfide from Hg(II)-thiolate complexes in natural organic matter. Environ. Sci. Technol. 49, 9787–9796.

Manceau, A., et al., 2016. Chemical forms of mercury in human hair reveal sources of exposure. Environ. Sci. Technol. 50, 10721–10729.

Manceau, A., et al., 2018. Biogenesis of mercury-sulfur nanoparticles in plant leaves from atmospheric gaseous mercury. Environ. Sci. Technol. 52, 3935–3948.

Manceau, A., et al., 2019. Mercury(II) binding to metallothionein in *Mytilus edulis* revealed by high energy-resolution XANES spectroscopy. Chem. Eur J. 25 (4), 997–1009.

Mathema, V.B., et al., 2011. Bacterial *mer* operon-mediated detoxification of mercurial compounds: a short review. Arch. Microbiol. 193 (12), 837–844.

Miklavčič, A., et al., 2013. Mercury in food items from the Idrija mercury mine area. Environ. Res. 125, 61–68.

Mindlin, S., et al., 2005. Present-day mercury resistance transposons are common in bacteria preserved in permafrost grounds since the Upper Pleistocene. Res. Microbiol. 156 (10), 994–1004.

Mlakar, I., 1974. An outline of production of the Idrija mercury mine through centuries (in Slovenian with English summary). Idrijski Razgledi 3–4 (XIX), 1–40.

Moore, D.M., Reynolds, R.C., 1989. X-ray Diffraction and the Identification and Analysis of Clay Minerals. Oxford University Press, Oxford.

Mulet, M., et al., 2015. *Pseudomonas alkylphenolica* sp. nov., a bacterial species able to form special aerial structures when grown on p-cresol. Int. J. Syst. Evol. Microbiol. 65 (11), 4013–4018.

Nascimento, A.M.A., Chartone-Souza, E., 2003. Operon *mer*: bacterial resistance to mercury and potential for bioremediation of contaminated environments. Genet. Mol. Res. 2 (1), 92–101.

Palinkaš, A.L., et al., 2008. Metallogeny of the northwestern and central dinarides and southern tisia. Ore Geol. Rev. 34, 501–520.

Petrova, M.A., et al., 2002. Mercury-resistant bacteria from permafrost sediments and prospects for their use in comparative studies of mercury resistance determinants. Russ. J. Genet. 38, 1569–1574.

Rasmussen, L.D., Sørensen, S.J., Turner, R.R., Barkay, T., 2000. Application of a *mer-lux* biosensor for estimating bioavailable mercury in soil. Soil Biol. Biochem. 32, 639–646.

Rovezzi, M., et al., 2017. High energy-resolution x-ray spectroscopy at ultra-high dilution with spherically bent crystal analyzers of 0.5 m radius. Rev. Sci. Instrum. 88 (1), 013108.

Rytuba, J., 2003. Mercury from mineral deposits and potential environmental impact. Environ. Geol. 43, 326–338.

Schué, M., et al., 2009. Sequence and analysis of a plasmid-encoded mercury resistance operon from *Mycobacterium marinum* identifies MerH, a new mercuric ion transporter. J. Bacteriol. 191 (1), 439-444.

Sahlman, L., et al., 1997. A mercuric ion uptake role for the integral inner membrane protein, MerC, involved in bacterial mercuric ion resistance. J. Biol. Inorg. Chem. 272 (47), 29518–29526.

Schiering, N., et al., 1991. Structure of the detoxification catalyst mercuric ion reductase from *Bacillus* sp. strain RC607. Nature 352 (6331), 168–172.

Serre, L., et al., 2004. Crystal structure of the oxidized form of the periplasmic mercury-binding protein MerP from *Ralstonia metallidurans* CH34. J. Mol. Biol. 339 (1), 161-171.

Silver, S., Hobman, J.L., 2007. Mercury microbiology: resistance systems, environmental aspects, methylation, and human health. In: Nies, D.H., Silver, S. (Eds.), Molecular Microbiology of Heavy Metals. Springer-Verlag, Berlin, Heidelberg, p. 357-370.

Steele, R.A., Opella, S.J., 1997. Structures of the reduced and mercury-bound forms of MerP, the periplasmic protein from the bacterial mercury detoxification system. Biochemistry 36 (23), 6885–6895.

Thomas, S.A., Gaillard, J.F., 2017. Cysteine addition promotes sulfide production and 4-fold Hg(II)-S coordination in actively metabolizing *Escherichia coli*. Environ. Sci. Technol. 51 (8), 4642–4651.

Thomas, S.A., et al., 2018. Spectroscopic and microscopic evidence of biomediated HgS species formation from Hg(II)–cysteine complexes: implications for Hg(II) bioavailability. Environ. Sci. Technol. 52, 10030–10039.

Tomiyasu, T., et al., 2017. The dynamics of mercury near Idrija mercury mine, Slovenia: horizontal and vertical distributions of total, methyl, and ethyl mercury concentrations in soils. Chemosphere 184, 244–252.

Wilson, J.R., et al., 2000. MerF is a mercury transport protein: different structures but a common mechanism for mercuric ion transporters? FEBS Lett. 472 (1), 78-82.

Wilson, K., 2001. Preparation of genomic DNA from bacteria. Current Protocols in Molecular Biology 56 (1), 2.4.1–2.4.5.